
*17th World Conference on Earthquake Engineering, 17WCEE*
*Sendai, Japan - September 13th to 18th 2020*

# PASSIVE HYBRID DAMPER WITH VARIABLE FORCE-DISPLACEMENT CHARACTERISTICS FOR SEISMIC PROTECTION OF STRUCTURES

K. K. Walsh[(1)] and K. Shirai[(2)]

[(1)] *Associate Professor, Department of Civil Engineering, Ohio University, walshk@ohio.edu*
[(2)] *Associate Professor, Faculty of Engineering, Hokkaido University, shirai.kazutaka@eng.hokudai.ac.jp*

## *Abstract*

Passive vibration control is one method that is effective for mitigating the response of, and reducing damage to, building or civil structures under seismic excitations. Recently, to achieve more enhanced control performance, several passive type devices with variable force-displacement characteristics have been proposed.

A passive variable friction damper (VFD) has been proposed that produces a decreased frictional force when the damper displacement exceeds a predetermined value. Also, a resetting passive stiffness damper (RPSD) has been proposed that produces a displacement-dependent damping force that resets to zero at each change in the damper direction.

In the present study, a novel hybrid system with passive variable damping force characteristics achieved by a parallel combination of VFD and RPSD for seismic protection of structures is proposed. A notable advantage of this hybrid system is that it produces a smart adaptable performance that is displacement-dependent despite its passive mechanism: demonstrating a high stiffness for decreasing structure displacements under small to moderate earthquakes; producing a constant force (i.e. zero tangential stiffness) with a magnitude that depends on the previous peak displacement after the high stiffness region of the force-displacement curve; and exhibiting a hardening effect when exceeding a predetermined displacement.

In this paper, an earthquake response analysis using a multi-degree-of-freedom linear building model incorporating the proposed hybrid system and subjected to a design input ground motion scaled to different intensities is presented. The obtained responses are compared with those of the VFD and RPSD alone, and without dampers. Through the numerical assessment, it is shown that the proposed hybrid system is effective in controlling the response of the structure under the design seismic excitation with several input magnifications.

*Keywords: passive control; hybrid damper; variable friction; resettable stiffness; displacement-dependent damping*



## 1. Introduction

Passive vibration control has been shown to be effective at reducing the response of seismically excited structures. In order to improve upon the performance of traditional passive dampers, new passive control devices with variable force-displacement characteristics have been proposed. Ribakov [1,2] developed a displacement-dependent friction damper that utilizes a wedge-form to increase the friction force in response to the damper displacement. The damper was shown to be effective at controlling the response of a seismically isolated and fixed-base seven-story structure. Shirai et al. [3] presented a displacement-dependent passive variable friction damper (VFD) that uses roller bearings pressed between tapered plates to decrease the damper force with increasing damper displacement. Dynamic loading of a full-scale steel structure showed that the damper exhibited stable operation and high endurance under cyclic loading. Another passive variable friction damper was proposed by Downey et al. [4,5] that used a parallel plate friction damper with a cam to produce a range of hysteretic behavior. It was shown through numerical analysis to be effective at controlling the response of a three-story building model subjected to both wind and seismic loading. Another passive variable damper proposed for multi-hazard protection of structures was the multiaction hybrid damper (MHD) [6], which used friction pads in series with lead rubber bearings (LRBs). The MHD was demonstrated to be effective at controlling the response of a twenty-story structure subject to wind loading, and a fifteen-story structure subject to seismic loading. Walsh et al. [7,8] investigated passive resettable stiffness using a rack-lever mechanism in combination with a mechanically operated valve. The force-displacement characteristics of the resetting passive stiffness damper (RPSD) were demonstrate through testing of a small-scale prototype, and numerical analysis showed that the damper was effective at controlling the response of a seismically excited base-isolated structure.

In the present study, a novel passive hybrid damper is presented that combines the VFD and RPSD to produce variable force-displacement characteristics. The hybrid damper exhibits high stiffness at small damper displacements, hardening at large damper displacements, and a constant damper force with a magnitude based on the previous peak damper displacement in between. The control effectiveness of the hybrid damper is examined through dynamic response analysis of a ten-story linear shear frame model subject to a design earthquake ground motion scaled to different intensities. The performance of the hybrid damper is compared to stand-alone VFDs and RPSDs designed to have the same peak damper force over a given range of damper displacements. The relative performances of the dampers are discussed in terms of their force-displacement characteristics and corresponding energy dissipation.

## 2. VFD+RPSD Hybrid Damper

The proposed hybrid damper combines the VFD with the RPSD to passively produce variable force-displacement characteristics. Consider the example hysteresis loop for the VFD shown in Fig. 1a. The force-displacement characteristics are defined by the peak damper force ($F_{peak}$) at zero damper displacement, zero damper force at the peak damper displacement ($x_{peak}$), and a linear change in the damper force in between. Meanwhile, the example hysteresis loop of the RPSD shown in Fig. 1b reveals that the damper generates a damping force that is proportional to the damper displacement, i.e. produces a small damping force at small displacement and large damping force at large displacements. When the stiffness of the RPSD is selected to be the ratio of the VFD peak force to peak displacement ($k_{rpsd}=F_{peak}/x_{peak}$), then parallel combination of the two dampers results in the example hysteresis loop of the proposed hybrid damper shown in Fig. 1c. The hysteresis loop of the hybrid damper is characterized by high initial stiffness due to the VFD, followed by a constant damping force due to the combination of the VFD+RPSD, and then a hardening effect due to the RPSD. Furthermore, the magnitude of the hybrid damper force depends on the previous peak damper displacement. The example hysteresis loop of the hybrid damper shown in Fig. 1c highlights the variable force-displacement characteristics of the damper force.



 



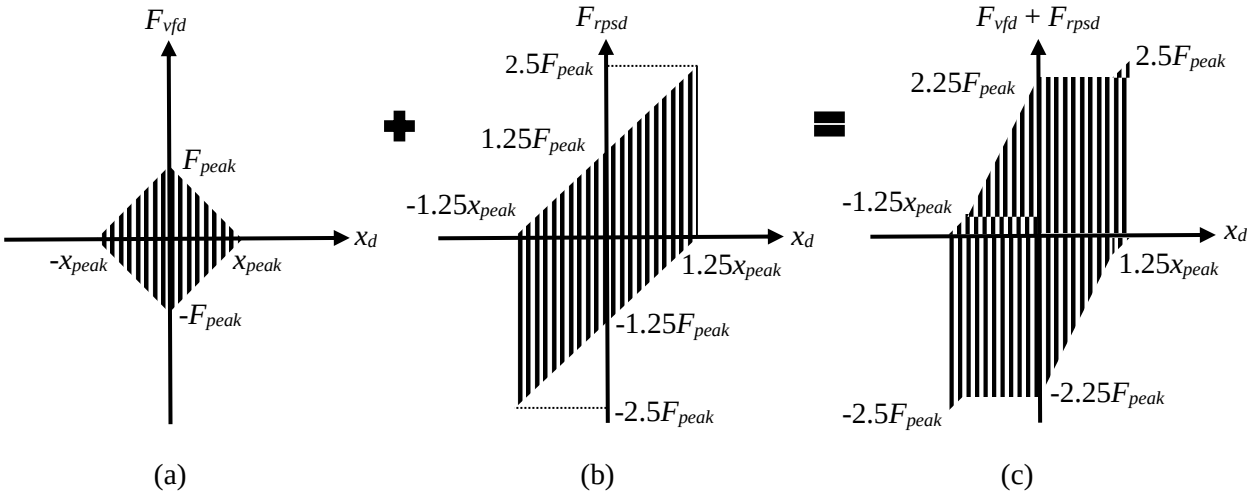


Fig. 1. Force-displacement characteristics of (a) VFD, (b) RPSD and (c) VFD+RPSD hybrid damper.

## 2.1 VFD description

The VFD utilizes a variable height component comprised of roller bearings situated between tapered sections of two plates [3] as shown in Fig. 2a. A third plate is located below the variable height component and supports a friction material. The upper plate of the variable height component and the third plate (supporting the friction material) are constrained to have the same displacement, while the lower plate of the variable height component can move independently. The three plates are connected using a disk spring and bolt set that compresses the variable height component and provides a high normal force on the friction material. As shown in Fig. 2b, as the lower plate of the variable height component displaces there are two mechanisms contributing to the variable friction force: (1) the lower plate of the variable height component slides along the friction material supported by the third plate, and (2) the roller bearings move down the tapered sections of the plates resulting in a decrease in the normal force on the friction material. Fig. 3 shows the hysteresis loop of a VFD combined with a traditional friction damper obtained through experimental testing of a full-scale steel frame [3]. The constant force near zero damper displacement, and the sloped portions of the curve at larger displacements, are directly related to the shape profile of the plates used in the variable height component of the damper.

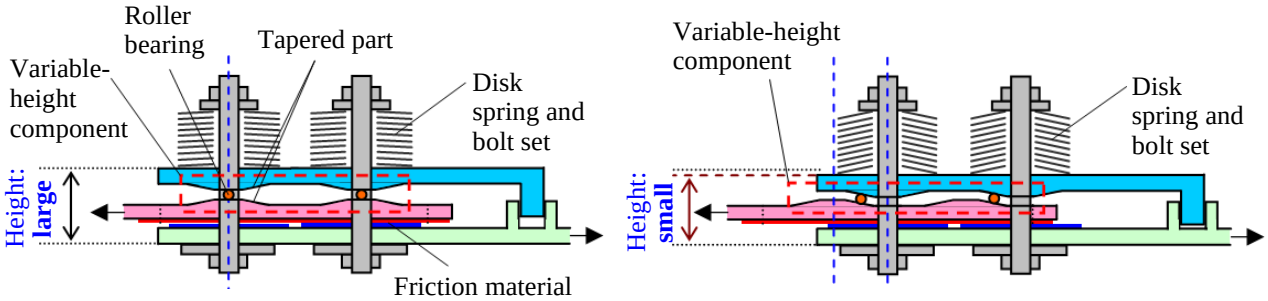


Fig. 2. VFD at (a) neutral position and (b) deformed position [3].



 



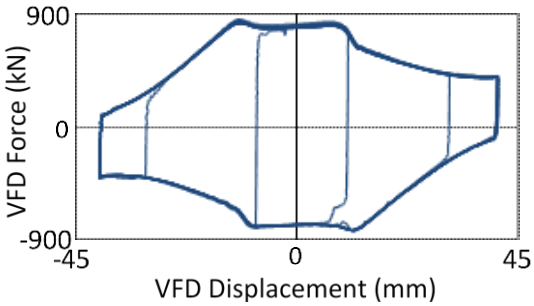


Fig. 3. Hysteresis loop of VFD combined with traditional friction damper [3].

### 2.2 RPSD description

A schematic of the RPSD [7] is shown in Fig. 4a. It consists of a gas-filled cylinder divided into two chambers connected with an external bypass loop. A mechanically operated, normally closed plunger valve on the bypass loop controls the flow of gas between chambers. Actuation of the mechanical valve is handled using a rack-lever mechanism comprised of a spring-loaded lever mounted in a vertical channel over a grooved rack, that is in turn connected to the damper piston. For each change in piston direction, the rack drives the lever up the vertical channel and engages the valve plunger, thereby opening the valve and resetting the damper force to zero. The valve remains open until the lever moves back down the channel and disengages the valve plunger, at which time the valve closes. Further action of the piston increases the force in the damper again. A hysteresis loop obtained from cyclic loading of a small-scale prototype RPSD [7] is shown in Fig. 4b. It can be seen from Fig. 4b that there is a delay in resetting of the damper force after each change in direction of the damper piston, followed by another delay before the force begins increasing again. The delay is due to the time takes for the lever to move up and down the channel to actuate the valve at each change in direction. These resetting delays can be minimized through proper selection of the valve and resetting mechanism components.

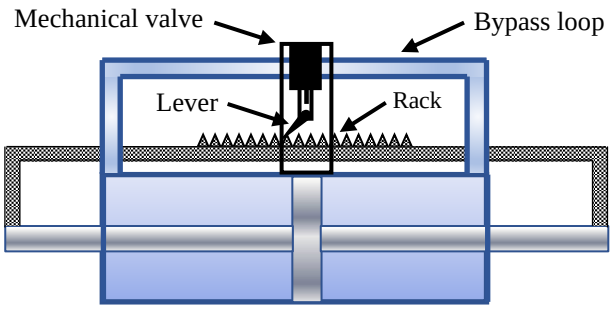


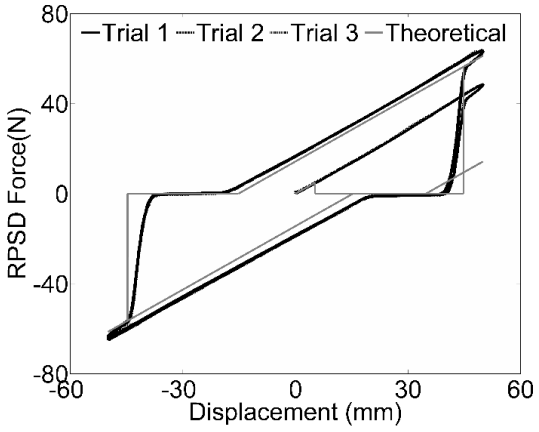


(a) (b)

Fig. 4. RPSD (a) schematic and (b) experimental hysteresis loop [7].

## 3. Dynamic Response Analysis

### 3.1 VFD model

The friction force in the VFD decreases with increasing positive and negative damper displacement and increases with decreasing positive and negative displacement. A simple model for describing the damper force as a function of the damper displacement is given as follows:



 



$$F_{vfd}(t) = sign(\dot{x}_{vfd}(t)) \cdot \left[F_{peak} - F_{peak} \cdot \frac{|x_{vfd}(t)|}{x_{peak}}\right], \quad (1)$$

where $F_{peak}$ is the damper force at zero damper displacement, $x_{peak}$ is the peak displacement at which the damper force is zero, and $x_{vfd}(t)$ is the damper displacement. For a VFD installed in a building structure using an elastic brace, the force in the brace can be described by:

$$F_b(t) = k_b \cdot x_b(t), \quad (2)$$

where $k_b$ and $x_b(t)$ are the elastic stiffness and deformation of the brace, respectively. Accounting for the interaction between the VFD and elastic brace requires an algorithm for updating the damper and brace forces and deformations based on the inter-story drift at the location on the structure where the damper is installed. The resulting force exerted on the structure by the VFD with elastic brace is referred to hereafter by $F^b_{vfd}(t)$.

### 3.2 RPSD model

For the present study, an idealized model of the RPSD was used in which the damper is assumed to behave as a resettable spring with instantaneous resetting of the spring force. The equations describing the RPSD force are given by:

$$F_{rpsd}(t) = k_{rpsd} \cdot \left[x_{rpsd}(t) - x_l\right] \quad (3)$$

and

$$x_l = x_{rpsd}(t) \quad when \quad \dot{x}_{rpsd}(t) = 0, \quad (4)$$

where $k_{rpsd}$ and $x_{rpsd}(t)$ are the RPSD damper effective stiffness and displacement, respectively, and $x_l$ is the damper displacement at the previous instance of resetting. For the RPSD installed in a building structure using an elastic brace, the interaction between the damper and brace during resetting is ignored, and the interaction otherwise is handled through the effective damper-brace stiffness. The corresponding damper force is given as:

$$F^b_{rpsd}(t) = k^b_{rpsd} \cdot \left[x_{rpsd}(t) - x_l\right], \quad (5)$$

where

$$k^b_{rpsd} = \frac{k_{rpsd} \cdot k_b}{k_{rpsd} + k_b}. \quad (6)$$

### 3.3 Linear Frame Model

For a linear *n*-story shear frame equipped with *m* VFD+RPSD hybrid dampers, the governing equation of motion is:

$$\mathbf{M_f}\ddot{\mathbf{x}}(t) + \mathbf{C_f}\dot{\mathbf{x}}(t) + \mathbf{K_f}\mathbf{x}(t) = \mathbf{E}\mathbf{F_e}(t) - \mathbf{D}(\mathbf{F^b_{vfd}}(t) + \mathbf{F^b_{rpsd}}(t)), \quad (7)$$

where $\mathbf{M_f}$, $\mathbf{C_f}$, and $\mathbf{K_f}$ are the *n* x *n* mass, damping, and stiffness matrices of the frame, respectively. The *n* x 1 vectors $\mathbf{x}(t)$, $\dot{\mathbf{x}}(t)$, and $\ddot{\mathbf{x}}(t)$ represent the horizontal displacements, velocities, and accelerations (relative to the ground) of each floor mass at time *t*. The matrix $\mathbf{E}$ is an *n* x *r* excitation location matrix for the *r* x 1 vector of excitation forces $\mathbf{F_e}(t)$, and the matrix $\mathbf{D}$ is an *n* x *m* location matrix for the *m* x 1 vectors of forces $\mathbf{F^b_{vfd}}(t)$ and $\mathbf{F^b_{rpsd}}(t)$ produced by the VFDs and RPSDs in combination with elastic braces, respectively. Equation (7) can also be expressed in state-space representation as:

$$\dot{\mathbf{z}}(t) = \mathbf{A}\mathbf{z}(t) + \mathbf{B}\mathbf{u}(t), \quad (8)$$

where



 



$$\mathbf{A} = \begin{bmatrix} \mathbf{0} & \mathbf{I} \\ -\mathbf{M_f^{-1}K_f} & -\mathbf{M_f^{-1}C_f} \end{bmatrix}, \mathbf{B} = \begin{bmatrix} \mathbf{0} & \mathbf{0} \\ \mathbf{M_f^{-1}E} & -\mathbf{M_f^{-1}}\boldsymbol{D} \end{bmatrix}, \mathbf{u}(t) = \begin{bmatrix} \mathbf{F_e}(t) & \left(\mathbf{F_{vfd}^b}(t) + \mathbf{F_{rpsd}^b}(t)\right) \end{bmatrix}^{\boldsymbol{T}}, \quad (9)$$

and

$$\mathbf{z}(t) = [\mathbf{x}(t) \quad \dot{\mathbf{x}}(t)]^{\mathrm{T}}. \quad (10)$$

### 3.4 Model inputs

The example structure chosen for this study was a linear 10-story shear frame with a fundamental period of 1.0 s and damping ratio of 2%. The properties of the frame are shown in Table 1. A single VFD+RPSD hybrid damper was assumed to be installed at each story of the frame using an elastic brace. The peak force of the VFD in the hybrid damper installed at the $i^{th}$ story was taken to be 2% of the building weight above the story ($F_{peak,i} = 0.02\sum_i^n w_i$) and the peak displacement was taken to be 40 mm ($x_{peak,i}$ = 40 mm). The stiffness of the RPSD in the hybrid damper installed at the $i^{th}$ story was determined such that the RPSD force at the peak displacement of the VFD would be twice the peak VFD force ($k_{rpsd,i} = F_{peak,i}/x_{peak,i}$). The stiffness of the elastic brace used to install the hybrid damper at the $i^{th}$ story was assumed to be equal to the story stiffness ($k_{b,i} = k_{f,i}$). The properties of the VFD and RPSD are shown in Table 1. The frame model with and without hybrid dampers was subjected to a simulated design earthquake ground motion scaled to magnification factors ranging from 0.25-2.50 (with a 0.25 increment). The time history and acceleration response spectrum (5% damping) for the unscaled ground motion, which was prepared in a previous study [9], is shown in Fig. 5. The response of the frame with the RPSD and VFD alone are also determined for comparison. The RPSD and VFD were designed to have the same peak force as the VFD+RPSD hybrid damper over the range of displacements $\pm x_{peak}$. This was achieved by using the same stiffness for the RPSD but doubling the peak force of the VFD ($F_{peak,i} = 0.04\sum_i^n w_i$).

Table 1. Model inputs for dynamic analysis of 10-story shear frame.

| Story | Height $H$ (m) | Mass $m_f$ (ton) | Stiffness $k_f$ (=$k_b$) (MN/m) | Damping coefficient $c_f$ (MN-s/m) | VFD Peak Force $F_{peak}$ (kN) | RPSD Stiffness $k_{rpsd}$ (kN/m) |
|---|---|---|---|---|---|---|
| 10 | 40 | 1000 | 1061.66 | 6.76 | 196.13 | 4903.33 |
| 9 | 36 | 1000 | 1179.63 | 7.51 | 392.27 | 9806.65 |
| 8 | 32 | 1000 | 1297.59 | 8.26 | 588.40 | 14709.98 |
| 7 | 28 | 1000 | 1415.55 | 9.01 | 784.53 | 19613.30 |
| 6 | 24 | 1000 | 1533.51 | 9.76 | 980.67 | 24516.63 |
| 5 | 20 | 1000 | 1651.48 | 10.51 | 1176.80 | 29419.95 |
| 4 | 16 | 1000 | 1769.44 | 11.26 | 1372.93 | 34323.28 |
| 3 | 12 | 1000 | 1887.40 | 12.02 | 1569.06 | 39226.60 |
| 2 | 8 | 1000 | 2005.36 | 12.77 | 1765.20 | 44129.93 |
| 1 | 4 | 1000 | 2123.33 | 13.52 | 1961.33 | 49033.25 |



 



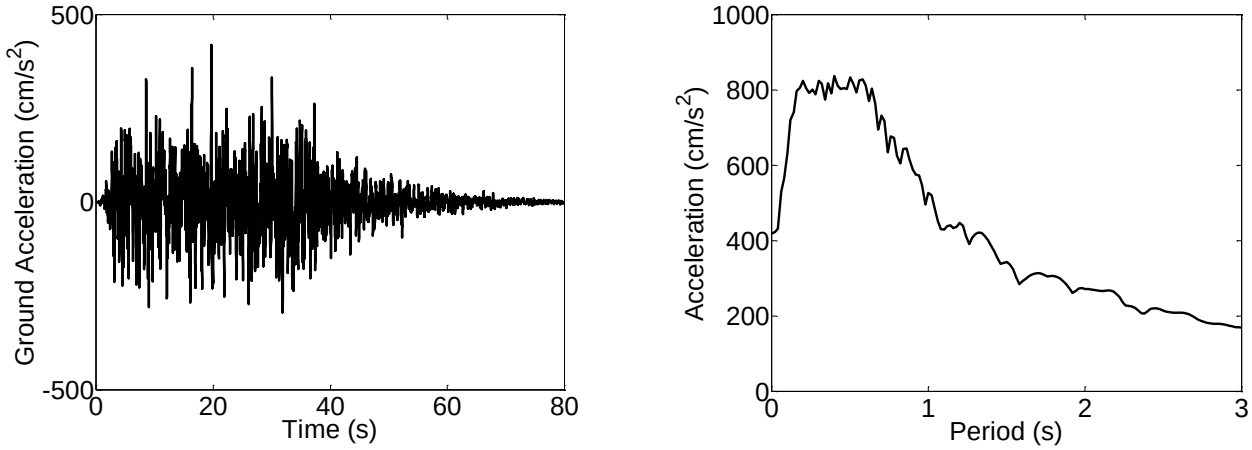


(a) (b)

Fig. 5. Design ground motion (a) time history and (b) acceleration response spectrum (5% damping).

## 4. Results and Discussion

The hysteresis loops for the VFD, RPSD, and VFD+RPSD hybrid damper at the third story of the frame and for an input magnification of 2.00 are shown in Fig. 6. Also included in the figure is the energy dissipated by each damper. Comparison of Fig. 6a-c shows that the VFD+RPSD dissipated the most energy, followed by the VFD, and then the RPSD. Fig. 6c highlights the variable force-displacement characteristics of the VFD+RPSD; high initial stiffness followed by a constant force with magnitude dependent on the previous peak displacement, and then a hardening effect at large displacement.

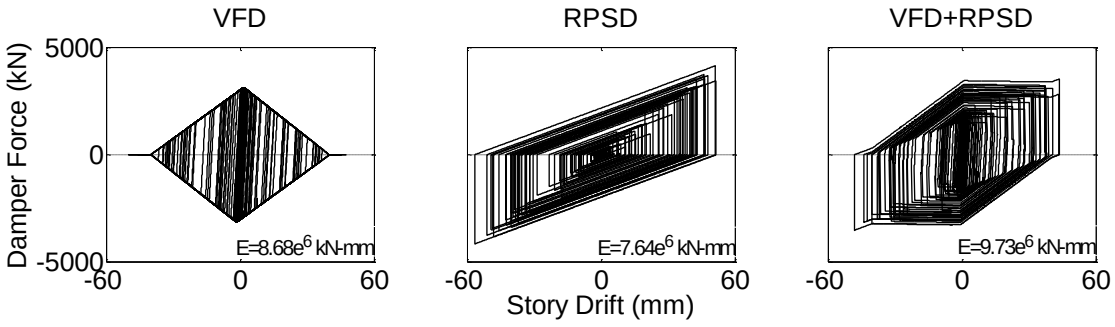


(a) (b) (c)

Fig. 6. Simulated hysteresis loops for the (a) VFD, (b) RPSD and (c) VFD+RPSD.

In order to compare the control performance of the three dampers, response ratios were calculated for the peak drift, absolute acceleration, and shear force (restoring force + damper force) at each story of the frame and for input magnifications representing low, moderate, and high intensity ground motions. The response ratios were calculated as the ratio of the response of the frame with dampers to the response of the frame without dampers, and therefore smaller response ratios indicate better control performance. The peak drift response ratios are plotted versus the story number in Fig. 7. All the response ratios were found to be less than unity, indicating that all three dampers reduced the drift response of the frame for the input magnifications considered. It is worth noting in Fig. 7 that the peak drift response ratios for the RPSD were the same at each story of the frame for all input magnifications. This can be attributed to the displacement dependent RPSD force, which increased proportionately with the story drift (i.e. input magnification).



 



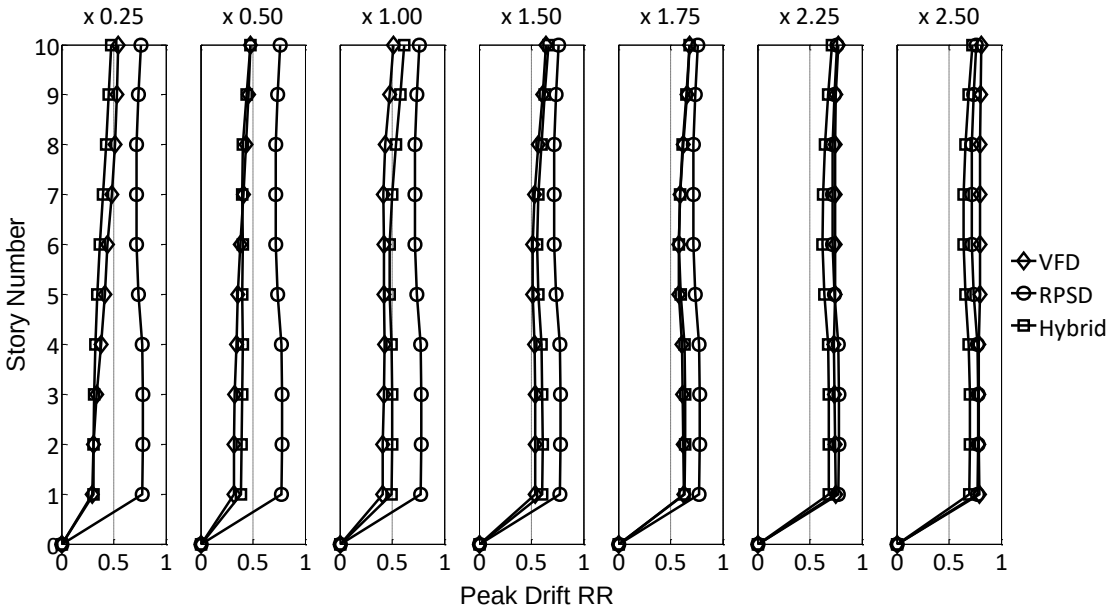


Fig. 7. Peak drift response ratios for each damper at different input magnifications.

Comparison of the peak drift response ratios in Fig. 7 shows that the VFD+RPSD yielded lower response ratios than the RPSD at all stories and for all input magnifications, but that the difference in response ratios decreased with increasing magnification. Meanwhile, comparison of the peak drift response ratios for the VFD+RPSD and the VFD shows that the dampers had similar response ratios at the lower and upper stories for input magnifications of 0.25 and 0.50, respectively. However, the VFD+RPSD yielded lower response ratios at the upper stories for magnification 0.25, and higher response ratios for the lower stories for magnification 0.50. For input magnification of 1.00, the peak drift response ratios for the VFD+RPSD were higher than those of the VFD at all stories, but the difference in the response ratios decreased with increasing magnification. At input magnification of 1.50 the response ratios were about the same at the upper stories, and at magnification of 1.75 they were almost identical at all stories. For the higher input magnifications of 2.25 and 2.50, the peak drift response ratios were smaller for the VFD+RPSD than the VFD at all stories, and the difference in response ratios increased with the magnification.

The peak absolute acceleration response ratios at each story of the frame and for the range of input magnifications considered are shown in Fig. 8. Once again it is observed that the response ratios for the RPSD at each story remained constant with increasing magnification. Comparison of the peak absolute acceleration response ratios for the VFD+RPSD hybrid damper and the RPSD shows that the VFD+RPSD almost always yielded smaller ratios than the RPSD. The largest difference in response ratios occurred at the smaller magnifications and the difference decreased with increasing magnification. The response ratios were not always smaller for the VFD+RPSD. Exceptions occurred at the first two stories for input magnifications 2.25 and 2.50, where the response ratios for the VFD+RPSD were greater than unity, i.e. peak acceleration increased relative to the frame with no dampers. This is attributed to spikes in the acceleration response that occurred during resetting of the RPSD force. These spikes did not lead to an overall increase in the frame response.



 



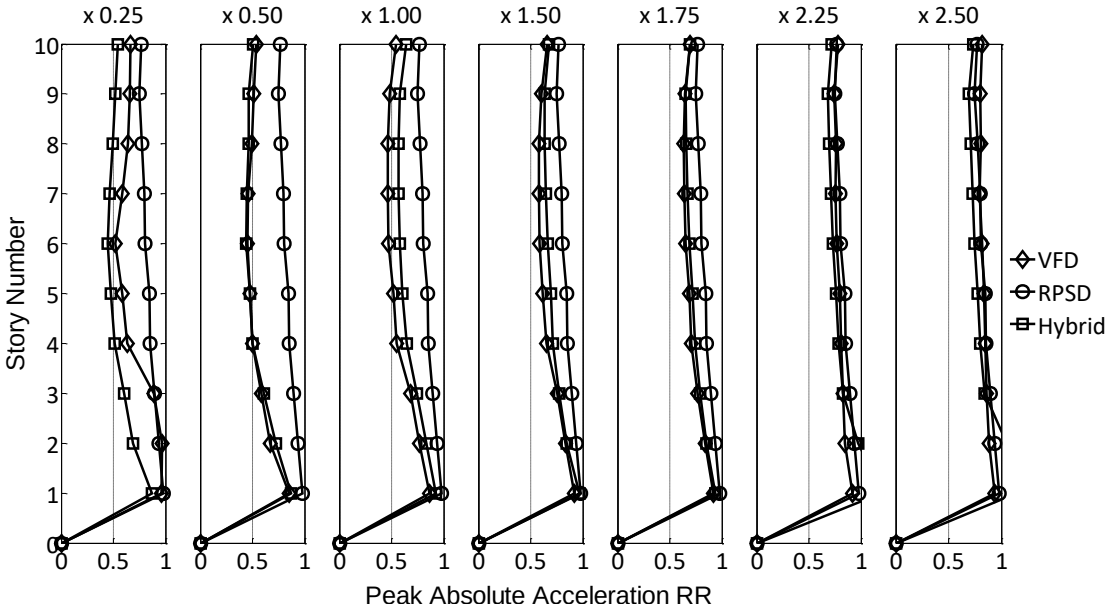


Fig. 8. Peak absolute acceleration response ratios for each damper at different input magnifications.

Comparison of the peak absolute acceleration response ratios in Fig. 8 shows that the ratios for the VFD+RPSD were smaller than those of the VFD at all stories for the 0.25 magnification, and approximately the same at all stories for the 0.50 magnification. As the input magnification was increased beyond 0.50, the response ratios for the VFD+RPSD became larger than those of the VFD initially, but the difference decreased with increasing magnification. At input magnification of 1.75 the response ratios for the two dampers were almost identical. When the input magnification increased to 2.25 and 2.50, the peak absolute acceleration response ratios were generally lower for the VFD+RPSD, and the difference in response ratios between the two dampers increased with increasing magnification. An exception occurred at the lower two stories of the frame where the response ratios for the VFD+RPSD were greater than unity.

The peak story shear (restoring force + damper force) response ratios for all three dampers are shown in Fig. 9 and were found to be practically identical to the peak drift response ratios for input magnifications 1.00-2.50. This is due to large restoring forces dominating the story shear at large drifts. At lower magnifications smaller peak story drifts resulted in smaller restoring forces, and the damper forces had a larger influence on the story shear. Furthermore, because the peak force of the VFD occurs at zero damper displacement, and the peak force of the VFD alone was twice that of the VFD in the VFD+RPSD hybrid damper, the peak story shear response ratios for the VFD+RPSD and VFD did not follow the same trend as the peak story drifts at input magnifications 0.25 and 0.50. Fig. 9 shows that the peak story shear response ratios for the VFD+RPSD were smaller than those of the VFD at all stories for input magnification of 0.25, and comparable at all stories for input magnification of 0.50.



 



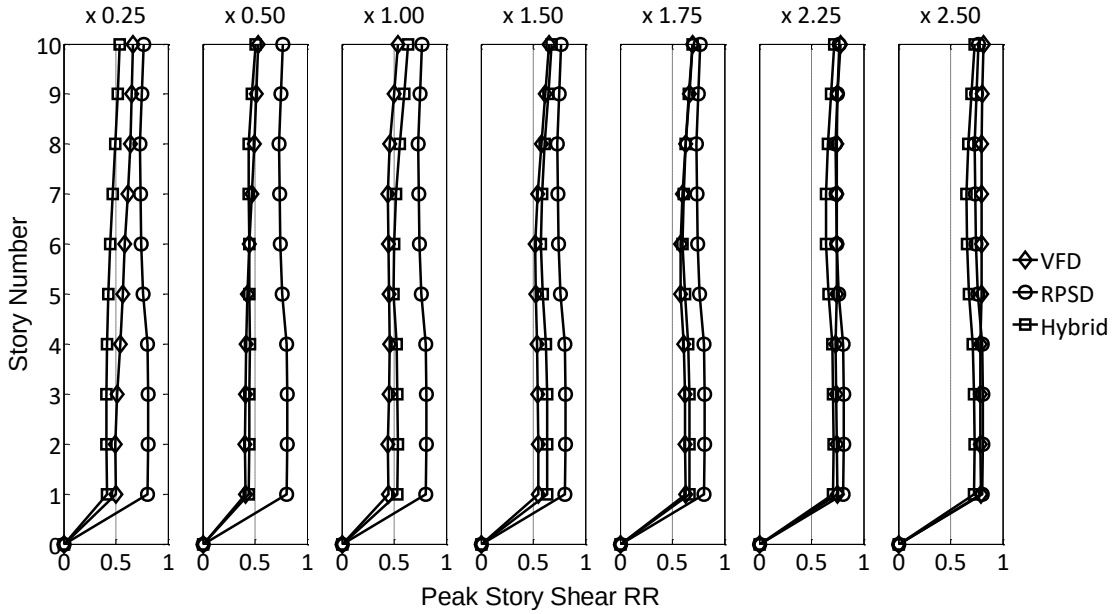


Fig. 9. Peak story shear response ratios for each damper at different input magnifications.

The results presented in Figs. 7-9 reveal a general trend regarding the relative performance of the VFD, RPSD, and VFD+RPSD hybrid dampers that is dependent on the intensity of the ground motion. For the lowest intensity ground motion, the RPSD forces were small, and its effectiveness in controlling the peak acceleration response of the frame was more comparable to that of the VFD+RPSD and VFD than its effectiveness in controlling the peak drift response. The small RPSD forces can be seen in Fig. 10 (see Fig. 10b), which represents the hysteresis loops for all three dampers at the first story of the frame and for the 0.25 input magnification. For the VFD, the forces were large for low intensity ground motions, as the peak damper force occurs at zero damper displacement. However, small damper displacements led to less friction damping and the damper behaved mostly as an elastic brace (see Fig. 10a). As a result, the VFD was more effective at controlling the drift response of the frame, but less effective at controlling the acceleration response. For the VFD+RPSD, the peak force of the VFD component was half that of the VFD alone, and friction damping was activated at smaller damper displacements. Therefore, the damper produced more friction damping and spent less time as an elastic brace (see Fig. 10c). The VFD+RPSD also had the contribution of the RPSD, albeit small for the low intensity ground motion. As a result, the VFD+RPSD was effective at controlling both the drift and acceleration response of the frame. Included in Fig. 10 is the energy dissipated by each damper. The VFD+RPSD and RPSD had comparable energy dissipation, which were an order of magnitude larger than the VFD. The RPSD had slightly larger energy dissipation than the VFD+RPSD, but at the cost of large story drifts due to small damper forces. Meanwhile, the energy dissipated by the VFD+RPSD was achieved through larger damper forces leading to smaller story drifts.

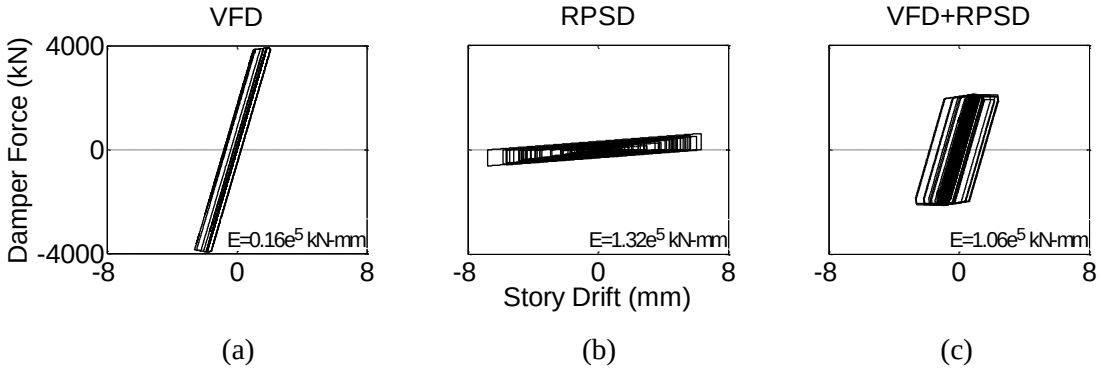


Fig. 10. Simulated hysteresis loops for the (a) VFD, (b) RPSD and (c) VFD+RPSD.



 



As the ground motion intensity increased from magnification 0.50-1.50, the effectiveness of the VFD in controlling both the drift and acceleration responses of the frame improved relative to the VFD+RPSD. This is due to an increase in friction damping as the drift response of the frame increased. As the intensity of the ground motion increased to between 1.75-2.50, the control performance of the VFD decreased relative to the VFD+RPSD. At these ground motion intensities, the peak story drifts were found to be approaching and exceeding the peak VFD damper displacements, beyond which no energy is dissipated by the device. Although the high intensity ground motions affected the VFD component of the VFD+RPSD damper the same way, they also led to an increase in the damper forces from the RPSD component, and significant energy was still dissipated by the hybrid damper. Figs. 7-9 show that the control performances of the VFD+RPSD and RPSD converged with increasing ground motion intensity, indicating that the RPSD component of the VFD+RPSD hybrid damper was playing an increasingly significant role in the damper performance.

To further examine the relationship between the ground motion intensity and damper performance, the total energy dissipated by all dampers in the frame was calculate for the VFDs, RPSDs and VFD+RPSDs. The results are plotted versus the entire range of input magnifications (i.e. 0.25-2.50 with 0.25 increments) in Fig. 11a. The total energy dissipated was lower for the RPSDs compared with the VFDs and VFD+RPSDs for all input magnifications except 2.50, where the energy dissipated by the RPSDs was slightly larger than that of the VFDs. The total energy dissipated by the RPSDs was smaller than, but comparable to, the energy dissipated by the VFDs at input magnification of 2.25. This is consistent with the control performance of the RPSD observed in Figs. 7-9, which resulted in response ratios that were generally larger than those of the VFD+RPSD for all magnifications, and generally larger than those of the VFD for all but magnifications 2.25 and 2.50.

Fig. 11a reveals that the total energy dissipated by the VFD+RPSDs was larger than the VFDs for input magnification 0.25, comparable for input magnifications 0.50-0.75, smaller for input magnifications 1.00-1.75, and larger for input magnifications 2.00-2.50. This is consistent with the relative control performance of these dampers observed in Figs. 7-9. Fig. 11a shows that the total energy dissipated by the VFDs decreased considerably relative to the VFD+RPSDs between input magnifications 1.75-2.50, for which the control performance of the VFD was found to decrease relative to the VFD+RPSD in Figs. 7-9. Fig. 11a also shows the total energy dissipation of the VFD+RPSDs and RPSDs converged at the higher input magnifications as more energy was dissipated by the RPSDs and the RPSD components of the VFD+RPSDs. The energy dissipation of the RPSD components of the VFD+RPSDs is further illustrated in Fig. 11b, which represents the total energy dissipated by the VFD and RPSD components relative to the total energy dissipated by the VFD+RPSD hybrid dampers. It shows that the total energy dissipated by the RPSD components exceeded that of the VFD components only at input magnifications above 2.00, and that below magnification of 2.00 most of the energy was dissipated by the VFD components.

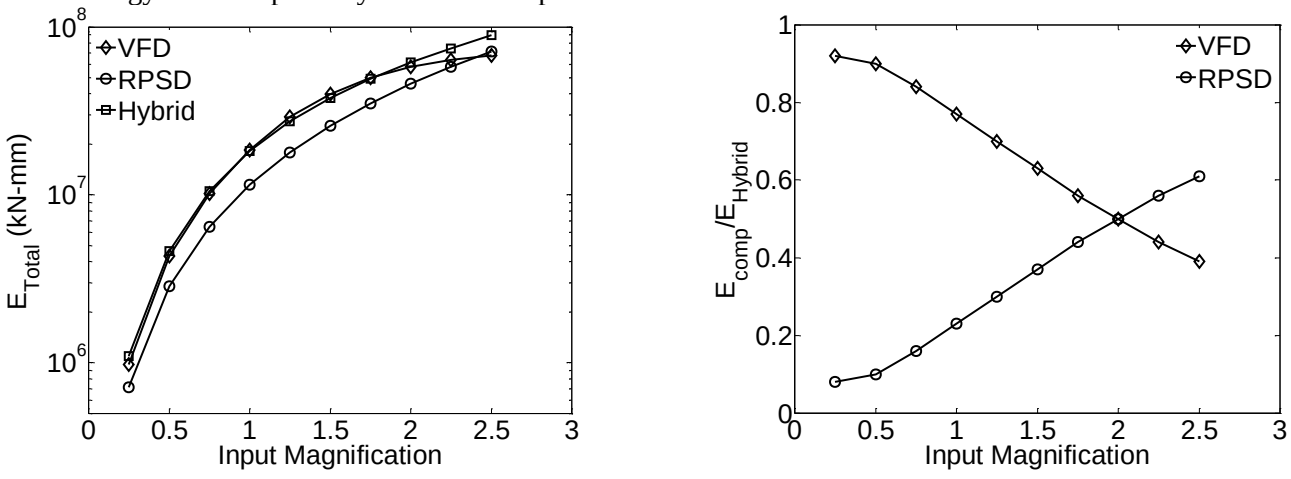


(a) (b)

Fig. 11. (a) Total energy dissipated and (b) ratio of hybrid damper component energy.



 



## 5. Summary and Conclusions

A novel hybrid damper that combines a passive variable friction device (VFD) with a resetting passive stiffness damper (RPSD) to passively achieve variable force-displacement characteristics was presented. The hybrid damper exhibits high stiffness at small damper displacements, hardening at large damper displacements, and a constant damper force with a magnitude based on the previous peak damper displacement in between. Dynamic response analysis was conducted to evaluate the effectiveness of the hybrid damper for controlling the response of a linear shear frame model subjected to a design ground motion scaled to different intensities. The performance of the hybrid damper was compared to a stand-alone VFD and RPSD designed to have the same peak damper force over a specified range of damper displacements. It was found that the control performance of the hybrid damper was generally superior to that of the RPSD at all ground motion intensities, superior to the VFD at the lowest and highest ground motion intensities, and comparable to the VFD at ground motion intensities in between. The relative performances of the three dampers was attributed to differences in their force-displacement characteristics and corresponding energy dissipation at the different ground motion intensities. It was observed that the hybrid damper benefited from the VFD component at small to moderate intensity ground motions and the RPSD component at large intensity ground motions, thereby highlighting the advantages of the proposed hybrid damping approach.

## 6. Acknowledgement

This study was supported by the JSPS KAKENHI Grant Number 19H02279.

## 7. References

[1] Ribakov Y (2010): Reduction of structural response to near fault earthquakes by seismic isolation columns and variable frictions dampers. *Earthquake Engineering and Engineering Vibration*, **9** (1), 113-122.

[2] Ribakov Y (2011): Using viscous and variable friction dampers for improving structural seismic response. *The Structural Design of Tall and Special Buildings*, **20** (5), 579-593.

[3] Shirai K, Sano T, Suzui Y (2013): Development of a passive variable friction damper with displacement-dependent damping force characteristics. *Proceedings of the Thirteenth East Asia-Pacific Conference on Structural Engineering and Construction (EASEC-13)*, Sapporo, Japan.

[4] Downey A, Sadoughi M, Cao L, Laflamme S, Hu C (2018): Passive variable friction damper for increased structural resilience to multi-hazard excitations. *Proceedings of the ASME 2018 International Design Engineering Technical Conferences and Computers and Information in Engineering Conference*, Quebec, Canada.

[5] Downey A, Theisen C, Murphy H, Anastasi N, Laflamme S (2019): Cam-based passive variable friction device for structural control. *Engineering Structures*, **188**, 430-439.

[6] Roh J, Hur M, Choi H, Lee S (2018): Development of a multiaction hybrid damper for passive energy dissipation. *Shock and Vibration*, https://doi.org/10.1155/2018/5630746.

[7] Walsh KK, Sallar G, Steinberg EP (2017): Modeling and Validation of a Passive Resettable Stiffness Damper. *Journal of Engineering Mechanics*, **143** (2), https://doi.org/10.1061/(ASCE)EM.1943-7889.0001190.

[8] Walsh KK, Sallar G, Steinber EP (2019): Hybrid base-isolation of a nonlinear building using a passive resettable stiffness damper. *Engineering Structures*, **178**, 206-211.

[9] Shirai K, Inoue N (2014): A seismic response estimation method for RC structures using random vibration theory. *Journal of Advanced Concrete Technology*, **12** (2), 62-72.



 